Surface-plasmon modes in Zn-doped InAs(001) and (111)

G. R. Bell and C. F. McConville*
Department of Physics, University of Warwick, Coventry CV4 7AL, United Kingdom

T. S. Jones
Department of Chemistry, Imperial College of Science, Technology and Medicine, London SW7 2AY, United Kingdom
(Received 5 June 1997)

We have investigated the plasmon modes present at the (001) and (111) surfaces of heavily doped *p*-type InAs, using high-resolution electron-energy-loss spectroscopy (HREELS) together with dielectric theory simulations. Two-dimensional electron plasmon modes are supported in the inversion layer close to the polar surfaces, however, these modes appear in the experimental HREEL spectra only as a broadening of the elastic peak due to their low energy. Deeper into the bulk, the hole plasma is characterized by light- and heavy-hole components supporting both optical and acoustic plasmon modes. Observation of the optical hole plasmon in HREELS allows the hole density profile to be estimated using dielectric theory simulations, which employ two plasma oscillators incorporating spatial dispersion to model the two-component hole plasma. It is found that native spatial dispersion cannot account for the pronounced experimental plasmon dispersion observed following argon-ion bombardment and annealing of the samples. This procedure is shown to cause rapid diffusion of the zinc acceptors into the near-surface region, resulting in large, highly nonuniform hole concentrations over the length scales probed by HREELS. The acoustic hole plasmon mode, which cannot normally be observed in specular HREELS, is discussed in terms of a two-oscillator, two-layer model. It is shown that acoustic modes do not contribute to specular HREEL spectra even in the limit of highly nonuniform charge distributions. [S0163-1829(97)04147-7]

I. INTRODUCTION

Surface-plasmon excitations have been the subject of continued investigation for many years, but only with the advent of high-resolution electron-energy-loss spectroscopy (HREELS) has it been possible to investigate the low-energy (10–100 meV) modes present in the near-surface region of doped semiconductors.[1] The dipole scattering process dominant in specular HREELS allows the wave vector of the plasmon to be altered simply by changing the incidence energy of the electron beam. Scattering can occur from plasmons localized well below the surface, and the effective probing depth of the beam is given approximately by the inverse of the plasmon wave vector. This typically lies in the range 100–1000 Å, making the technique ideal for probing inhomogeneous charge distributions in the near-surface region of materials,[1–4] although the combined effects on the experimental spectra of changes in both wave vector and probing depth must be separated.

By far the majority of HREELS studies of III-V semiconductor materials have focused on electron plasmon excitations. Hole plasmon excitations have been studied in GaAs(110),[5–7] however, there are no reported studies of the polar surfaces of *p*-type materials. The doping of InAs with Zn is of particular interest for two reasons; (i) there is a high density of donorlike surface states at polar surfaces which form a narrow inversion layer in *p*-type material, and (ii) the diffusion behavior of Zn in InAs is already well established.[8]

This paper is concerned with an HREELS study of the plasmon modes present at the (001) and (111) surfaces of Zn-doped *p*-type InAs. The near-surface region presents a complex distribution of three carrier types, namely electrons in an inversion layer, along with both light and heavy holes in the bulk. The electron plasma in the inversion layer supports a two-dimensional (2D) plasmon mode whose energy varies as the square root of the wave vector. The two-component hole plasma supports two distinct plasmon modes: an optical plasmon and an acoustic plasmon with linear dispersion. The acoustic hole plasmon dispersion cannot be observed in specular HREELS because of its linear dispersion relation, which does not intersect the line of constant phase velocity defined by the dipole scattering conditions. However, the possibility of observing a structure-induced acoustic plasmon in a highly nonuniform system is discussed below.

II. EXPERIMENTAL DETAILS

The experiments were carried out in a conventional ultra-high vacuum chamber [base pressure $\sim(1-2)\times10^{-10}$ mbar] equipped with low-energy electron diffraction (LEED), HREELS, an argon-ion gun, and an atomic hydrogen source. HREEL spectra were obtained in specular scattering geometry ($\theta_i=\theta_s=45°$) and with an instrumental broadening of 7–11 meV full width at half maximum (FWHM). Sample temperatures were measured by a cromel-alumel thermocouple in direct contact with the sample. The samples of Zn-doped InAs ($p\sim1\times10^{17}$ cm^{-3}) were mechanically polished and etched by the manufacturer (MCP Electronic Materials Ltd., UK) and loaded directly into the chamber with no further pretreatment. Note that the heavy-hole plasma frequency associated with a bulk doping level of $p\sim1\times10^{17}$ cm^{-3} is only 15 meV.

Clean surfaces were prepared either by atomic hydrogen

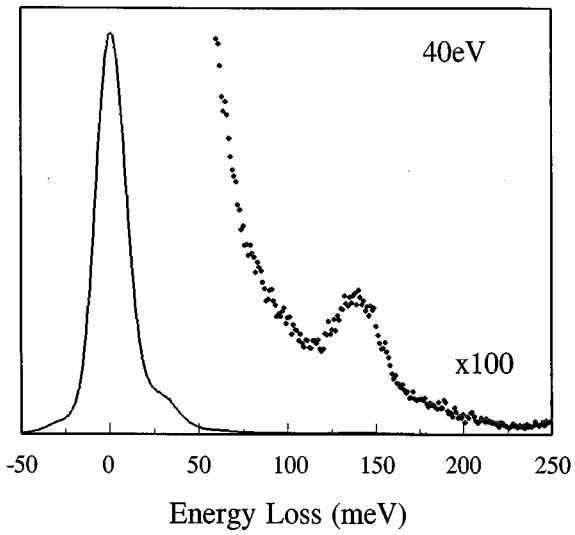

FIG. 1. A specular HREEL spectrum obtained from partially hydrogen-cleaned p-type InAs(111) using an electron energy of 40 eV. A shoulder on the wing of the elastic peak is visible, extending to approximately 35 meV, and a weak though distinct peak is seen at a loss energy of 139 meV in the expanded spectrum (dotted curve, $\times 100$ vertical scale).

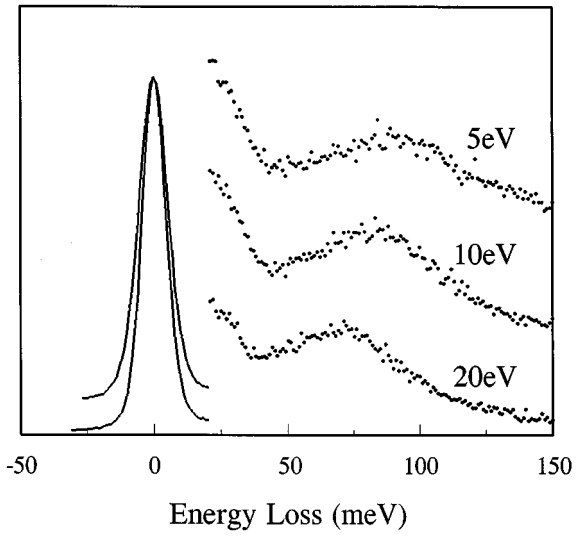

FIG. 2. A series of normalized HREEL spectra obtained from p-type InAs(111) prepared by IBA (ion energy 400 eV, polar incidence angle 60°). The higher loss energy region is shown as a set of expanded ($\times 10$) and vertically offset dotted curves for electron energies of 5, 10, and 20 eV, while the elastic peaks for electron energies of 5 and 20 eV are shown as solid curves (not offset).

cleaning[9] (AHC) or by cycles of low-energy ion bombardment and annealing (IBA).[10] To obtain clean and ordered surfaces by AHC, the samples were exposed to ~ 50 kL of molecular hydrogen flowing through the atomic hydrogen source (H_2 to $2H^*$ conversion efficiency $\sim 7\%$, $1\ \text{kL} = 10^{-3}$ torr s) at a sample temperature of 570 K. This procedure took about 20 min and resulted in the appearance of a sharp (4×1) LEED pattern on the (001) samples, and a sharp (2×2) pattern on the (111) samples. Sample preparation by two 20 min cycles of IBA produced the same LEED results, although it was found that subsequent IBA treatment produced large ($\sim 1\ \mu$m) clusters of indium droplets on the surface which were observed by both optical and atomic force microscopy (AFM). Samples were annealed to 550 K, and both the ion energy and angle of incidence were varied (400–2000 eV and grazing to normal incidence, respectively). Oxygen and carbon contamination was undetectable using Auger electron spectroscopy (AES) on samples prepared by both AHC and IBA, except after the highest-energy bombardment and annealing (2 keV). Samples treated in this way appeared slightly cloudy after extended annealing at 550 K, and some indium clustering was observed by AFM. The cloudy appearance of the samples coincided with the appearance of a small oxygen peak in AES spectra.

III. RESULTS

A specular HREEL spectrum (incidence energy $E_i = 40$ eV) obtained from p-type InAs(111) exposed to 10-kL H_2 at 570 K is shown in Fig. 1. There is a pronounced shoulder on the loss-side wing of the elastic peak, which is itself broadened (18-meV FWHM) beyond the nominal instrumental resolution (7-meV FWHM). The shoulder and elastic peak broadening result from collective excitations, namely the surface optical-phonon mode, the free-carrier plasmon modes, and coupled modes of the two. The spectrum is nearly featureless at higher loss energies, apart from a single peak at a loss energy of 139 meV. This peak disappeared for molecular hydrogen exposures of 50 kL or more, and also became more intense at lower incidence energies. It is assigned therefore to a contaminant vibrational mode of the partially cleaned surface[9] [a similar mode has been observed on partially hydrogen cleaned GaSb(001) (Ref. 11)]. The (001) surfaces were also prepared using AHC, and very similar spectra were obtained. However, the elastic peak broadening was significantly less (typically 12-meV FWHM at a nominal instrumental resolution of 7-meV FWHM). The overall shape of the broadened elastic peak and the shoulder was independent of annealing after full hydrogen cleaning, even for long annealing times (3 h) at over 600 K.

HREEL spectra for (111) surfaces prepared by IBA were very different from those of the hydrogen cleaned surfaces. Three typical spectra are shown in Fig. 2, obtained from a sample prepared by IBA with 400-eV argon ions incident at 60° to the surface normal. The stacked curves on the right (solid circles) show the higher-energy-loss regions for electron energies of 5, 10, and 20 eV, while the solid lines show the elastic peak region at $E_i = 5$ eV (top) and $E_i = 20$ eV (bottom) on the same vertical scale. There is clearly still significant elastic peak broadening (instrumental resolution was ~ 7 meV FWHM) which is slightly greater at $E_i = 5$ eV (14-meV FWHM) than at $E_i = 20$ eV (12-meV FWHM). In the higher loss region, a single extremely broad peak can be seen which shifts down in loss energy as the incidence energy is raised. The loss intensity peaks at around 85 meV for $E_i = 5$ eV, dropping to 71 meV for $E_i = 20$ eV, and it is assigned to the optical hole plasmon mode. Clearly, the carrier concentration in the near-surface region must be significantly greater than the nominal bulk doping level, for which the plasma frequency is 15 meV. There is also a pronounced

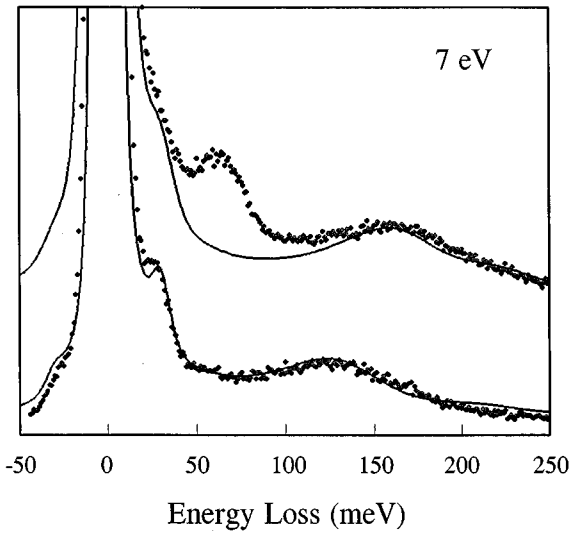

FIG. 3. Experimental (circles) HREEL spectra obtained from p-type InAs(001) surfaces prepared by IBA (ion energy 500 eV in the lower spectrum, 2 keV in the upper spectrum) using an electron energy of 7 eV. Simulated curves (solid lines) were generated using the three-layer dielectric model described in Sec. IV. The peak in the upper spectrum at 60 meV is not reproduced by the dielectric simulations.

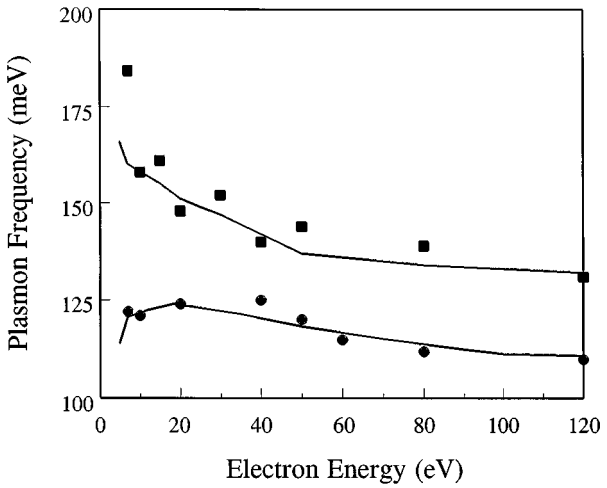

FIG. 4. The hole plasmon frequency plotted as a function of the electron incidence energy E_i for p-type InAs(001) samples prepared by IBA. In the upper curve (squares) the ion energy was 2 keV, while in the lower curve (circles) it was 500 eV, and in both cases the ions were incident at $\sim 30°$ to the surface normal. The solid lines are based on dielectric simulations (Sec. IV). The wave vector varies approximately as the inverse square root of the electron energy, e.g., for a 130-meV excitation energy, the inverse wave vector is 66 Å at 10 eV and 230 Å at 120 eV.

elastic peak shoulder in the loss energy region 20–40 meV which is more intense at lower electron incidence energies. Similar spectra were obtained for different IBA conditions, although there was a pronounced dependence of the optical hole plasmon frequency on the ion incidence angle. At grazing incidence, the hole plasmon was only visible as a long tail on the elastic peak, whereas at normal incidence, the loss intensity peaked at energies greater than 100 meV (although still with pronounced downward dispersion at higher electron energies).

Figure 3 shows two HREEL spectra (solid circles), recorded with electron energies of 7 eV, obtained from the (001) surface of p-type InAs prepared by IBA. The solid lines are theoretical spectra produced by dielectric theory simulations (see Sec. IV). In both cases, the ions were incident at 30° to the surface normal and the samples were annealed to 550 K. The upper spectrum corresponds to an ion energy of 2 keV, while the lower spectrum corresponds to an ion energy of 500 eV. In both spectra there is a very broad peak at high loss energies (centered at 184 and 124 meV for the upper and lower spectra, respectively). These peaks exhibit pronounced dispersion, similar to the broad peaks shown in Fig. 2 for the (111) surface, and they are again assigned to the optical hole plasmon mode. The dispersion is shown over a wide range of electron energies (7–120 eV) in Fig. 4 and in both cases the overall trend is downwards with increasing electron energy. The upper curve (solid squares) indicates the dispersion of the optical hole plasmon for the sample bombarded at 2-keV ion energy, while the lower curve (solid circles) corresponds to an ion energy of 500 eV. The solid curves were produced by dielectric theory simulations. Note that the overall dispersion is much greater for the higher-energy ion bombardment (an overall shift of ~ 42 meV for the 2-keV bombarded sample, compared with ~ 20 meV for the 500-eV sample).

There is also a shoulder visible on the elastic peaks of both spectra shown in Fig. 3, better defined on the lower spectrum due to improved instrumental resolution, which extends to a loss energy of 28 meV. This is the surface optical-phonon excitation, and its intensity decreases as the electron energy is increased. The peak at 60 meV is not reproduced by the theoretical curve. This peak was observed only for the highest ion energy employed (2 keV) and after extended annealing at 550 K. Samples subjected to this IBA treatment appeared slightly ''cloudy,'' and some oxygen contamination was detected in AES. The peak intensity decreased strongly as the electron energy was raised, and it was hardly detectable at $E_i = 20$ eV. The dispersion of the peak was estimated by subtracting simulated curves from the experimental curves, and it was found that the peak stayed at a constant loss energy of 60 meV. The lack of dispersion is characteristic of a surface vibrational mode, and so the loss peak is assigned to an oxide-related vibrational mode on the damaged and indium-rich surface.

IV. BAND STRUCTURE AND DIELECTRIC MODELING

The valence-band structure of InAs was modeled as parabolic light- and heavy-hole bands with constant effective masses of $0.025m_e$ and $0.41m_e$, respectively (where m_e is the free-electron mass). The density of occupied states in each band was calculated as a function of the overall hole concentration p, and light-hole and heavy-hole plasma frequencies $\omega_{\rm lh}$ and $\omega_{\rm hh}$ were calculated separately for each hole gas. The plasma frequencies are shown as a function of the total hole concentration in Fig. 5. In the carrier-concentration regime of interest ($p \sim 10^{18} - 10^{19}$ cm^{-3} in the near-surface region, as determined from fitting of the experimental data) and at room temperature ($k_B T \sim 26$ meV), the

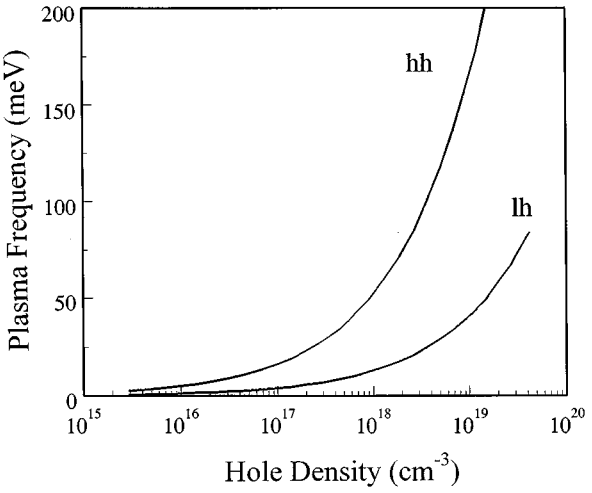

FIG. 5. The calculated light-hole (lh) and heavy-hole (hh) plasma frequencies for InAs at room temperature plotted as a function of the total hole concentration, based on parabolic bands with effective masses of $0.0025m_e$ and $0.41m_e$, respectively.

bands are partly degenerate with the Fermi level lying ~ 15 meV below the valence-band maximum.

The schematic band alignment and a corresponding three-layer dielectric model are shown in Fig. 6. The conduction band is expected to become degenerate close to the surface due to the presence of a high density of electrons donated from surface defects.[12–14] Beyond this inversion layer, the samples are assumed to become strongly p-type, consistent with the very high plasma frequencies observed in HREELS. Inhomogeneity in the hole density profile in the near-surface region is accounted for by the presence of the ''mid-layer,'' while the inversion layer is treated as carrier free (a ''dead layer''). The reasons for the latter approximation are given in Sec. V B. Deep into the bulk, the carrier concentration should approach the nominal bulk doping level of 1×10^{17} cm^{-3}, where the valence bands are nondegenerate. However, HREELS can only probe the upper few hundred angstroms of the sample, and so the ''bulk'' carrier concentration in the dielectric model is not constrained to be equal to the true bulk doping level. In Fig. 6, the valence band is shown as degenerate in the mid-layer and nondegenerate in the ''bulk'' region, in accordance with the experimental findings detailed later.

In the mid-layer ($i=2$) and bulk ($i=3$), the dielectric function is assumed to be of the form

$$\varepsilon_i(q,\omega)=\varepsilon(\infty)\left[1+\frac{\omega_{\rm ph}^2}{\omega_{\rm TO}^2-\omega^2-i\gamma\omega}-\frac{\omega_{\rm hi}^2}{\omega^2-\beta_{\rm hi}^2q^2+i\Gamma_h\omega}-\frac{\omega_{\rm li}^2}{\omega^2-\beta_{\rm li}^2q^2+i\Gamma_1\omega}\right], \quad (1)$$

where the first two terms in the square brackets account for the lattice response of the material, and the last two terms account for the hole gas response. The high-frequency dielectric constant $\varepsilon(\infty)$ is set at 12.25.[15] The optical-phonon term contains the phonon strength ($\omega_{\rm ph}$), transverse-optical-phonon frequency ($\omega_{\rm TO}$), and phonon damping (γ) in the

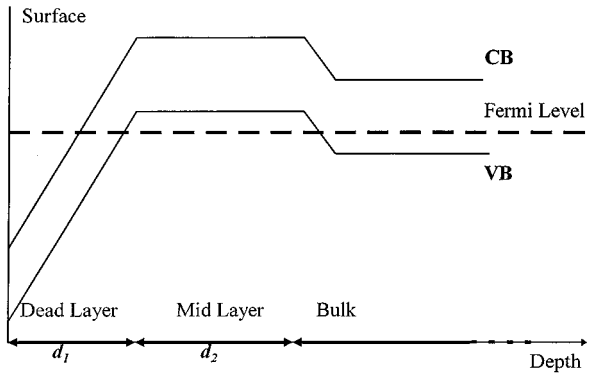

FIG. 6. A schematic diagram of the band line-up near the surface of p-type InAs samples prepared by IBA, showing the degenerate n-type inversion layer at the surface, a middle region which is degenerately p-type, and a p-type bulk region. The corresponding layer thicknesses d_1 and d_2 for the three-layer dielectric model are shown on the horizontal axis.

usual way.[3,10] The two hydrodynamic plasma terms correspond to the heavy- and light-hole gases, respectively. In each of the two plasma active layers, there is a plasma frequency for each hole type ($\omega_{\rm hi}$ and $\omega_{\rm li}$, $i=2,3$) and also a spatial dispersion term for each hole type ($\beta_{\rm hi}$ and $\beta_{\rm li}$, $i=2,3$). In the partly degenerate system studied here, the Debye-Hückel model was used to calculate the spatial dispersion terms for each of the four plasma oscillators (the Thomas-Fermi values were also derived and were somewhat smaller for all the carrier concentrations considered). The plasmon wave vector q can be calculated for a given dipole scattering event, and increases as the electron energy is reduced.[3] The plasmon damping factor Γ_h was a free parameter in the simulations, and Γ_1 was constrained to be greater by a factor $(m_h/m_l)^{1/2}$ to take into account the higher rate of ionized impurity scattering for the faster carrier species. However, independent changes in the light-hole plasmon damping had only minor effects on the simulated spectra compared with the effects of the heavy-hole damping parameter.

HREEL spectra were simulated using the approach of Lambin, Vigneron, and Lucas[16] modified to incorporate the two-oscillator plasma dielectric function given in Eq. (1). For each sample, experimental spectra obtained using a wide range of electron incidence energies (5–120 eV) were simulated to derive a single set of best-fit parameters. This procedure ensures that a wide variety of effective probing depths and plasmon wave vectors are sampled. All of the model parameters were fixed for a given set of experimental data, except for the plasmon damping, which was allowed to vary as a function of electron incidence energy to account for the various plasmon damping mechanisms.[7,17,18] It was found that high plasmon damping ($\Gamma\sim\omega$) was required in all of the spectra to reproduce the large width of the plasmon peaks, and that the damping values were larger for spectra recorded with low incident electron energies.

V. DISCUSSION

A. Dopant diffusion and IBA effects

The diffusion behavior of Zn in InAs has been widely studied,[8] and the low activation energy ΔE for diffusion

($\sim$1.2 eV) and high diffusion constant D_0 ($\sim 3\times10^{-3}$ $cm^2\,s^{-1}$) means that the diffusion process can be more readily observed than in most III-V impurity systems. Detailed calculations were not performed here due to the complexities of the system (such as a concentration-dependent diffusion coefficient arising from a switch in the dominant diffusion mechanism at a concentration of around 5×10^{18} cm^{-3}).[8] However, a simple calculation of the diffusion length x for a time $t=1$ h,

$$x\approx\sqrt{D_0 t}e^{-\Delta E/2k_BT}, \tag{2}$$

results in values of $x\sim0.05$ Å at room temperature and $x\sim0.15$ μm at the annealing temperature of 550 K. Clearly, the length scale for diffusion is very much less than the space-charge region probed by HREELS at room temperature, but is significantly greater during annealing. We assume therefore that the final dopant profile is limited solely by the driving force for diffusion rather than the diffusion process itself.

For both the (001) and (111) hydrogen cleaned surfaces, there is no distinct hole plasmon peak visible in the HREEL spectra, only a shoulder on the elastic peak together with some elastic peak broadening (Fig. 1). Even after extended annealing, no hole plasmon peak was observed, and so it can be concluded that significant Zn diffusion to the near-surface region does not occur. Dielectric theory simulations suggest that a near-surface hole concentration $\geqslant1\times10^{18}$ cm^{-3} would be necessary for the observation of a distinct hole plasmon peak in the experimental spectra. In contrast to the hydrogen cleaning process, IBA leads to the observation of hole plasmon frequencies between 70 and 180 meV (Figs. 2 and 3), implying near-surface hole concentrations in the range $2\times10^{18}-1\times10^{19}$ cm^{-3}. Clearly, significant diffusion to the surface region has occurred during the post-bombardment annealing cycle.

The spatial distribution of holes can be investigated by altering the electron incidence energy in HREELS. At higher electron energies, modes localized deeper in the bulk can scatter the probing electrons because of the smaller wave-vector transfer, leading to the concept of an energy-dependent ''effective probing depth.''[1] If the hole concentration decreases deeper into the bulk, the local plasma frequency will also drop. Higher-energy electrons will therefore sample a lower average plasma frequency, leading to a contribution to the plasmon dispersion (as a function of electron energy) additional to the native spatial dispersion. This mixture of two sources of dispersion generally means that simulations are needed to model the observed dispersion correctly. It should be noted that the effective probing depth is very approximate, and it is normally only possible to derive general features of the carrier profile. The simple three-layer model employed here is only a schematic representation of the true profile.

In previous papers, we have investigated the effects of IBA on the near-surface region of both InAs(001) (Ref. 10) and InSb(001).[19] In both cases, significant n-type doping is produced in the upper $\sim$1000 Å region of the sample due to ion-induced defects. For InAs, we have shown that the amount of damage induced in the sample, as measured by the additional *electron* concentration using HREELS, depends critically on the ion sputtering conditions employed.[10] In particular, damage is minimized at grazing incidence and low ion energies. The results presented here show a similar trend since at grazing incidence, the additional *hole* concentration is minimized, while it is greatest for high-energy bombardment fairly close to normal incidence (Figs. 3 and 4). We conclude therefore that the driving force for Zn diffusion into the near-surface region is the residual ion-induced damage produced during bombardment which leaves a very high defect density close to the surface. These provide sites for Zn atoms, which during annealing become sufficiently mobile to occupy these sites. Dopant diffusion is essential for the observation of these high hole concentrations: for example, for p type InSb (Cd-doped, $p\sim10^{14}$ cm^{-3}), IBA induces n-type behavior near the surface[19] because dopant diffusion is negligible in this system.[8]

TABLE I. The parameters used in the three-layer dielectric model to produce best fits to two sets of the experimental HREEL spectra obtained from p-type InAs(001) prepared by IBA. In both cases the samples were bombarded at an angle of 30°, and the ion energy was either 2 keV or 500 eV. The parameters are the mid-layer thickness (d_2) and hole concentration (p_2), the bulk hole concentration (p_3) and the dead layer thickness (d_1).

Ion energy	p_2 (cm^{-3})	p_3 (cm^{-3})	d_1 (Å)	d_2 (Å)
2 keV	3×10^{19}	4×10^{18}	32	49
500 eV	2×10^{19}	4×10^{18}	35	33

By fitting the HREEL spectra and the observed optical hole plasmon dispersion using the dielectric theory, it was possible to estimate the carrier profile close to the surface. Theoretical curves are shown in Fig. 3 for the (001) surface prepared by different IBA procedures (although fits for only the 7-eV spectra are shown, similar fits were generated across the whole range of incidence energies). Clearly they fit the experimental curves very well, with the exception of the 60-meV loss peak evident in the upper spectrum (ion energy equals 2 keV). In particular, the optical hole plasmon peak is reproduced by the two-oscillator plasma dielectric function employed. The dramatic dispersion of the hole plasmon peaks for these samples is shown in Fig. 4 with the solid lines representing fits to the dispersion curve generated by the dielectric model. Again, the fits are extremely good (note the error in the peak position for the extremely broad plasmon peaks is several meV), with the models used to produce the fits containing a mid-layer (layer 2) with a significantly higher plasma frequency than the bulk layer, indicating a very strong inhomogeneity in carrier concentration across the region probed by HREELS. The carrier concentrations in each of the layers for both surfaces are shown in Table I, together with the mid-layer thickness (d_2) and the dead layer thickness (d_1). For both samples, the carrier concentration inferred in the mid-layer is almost an order of magnitude higher than the ''bulk'' carrier concentration. This very sharp inhomogeneity was required to model the observed dispersion of the hole plasmon (Fig. 4), with the spatial dispersion of the plasma taken into account. The main difference between the two systems is that for the 2-keV bombarded sample, the mid layer is slightly thicker (49-Å compared with 33 Å) and has a slightly higher carrier con-

centration (3×10^{19} cm^{-3} compared with 2×10^{19} cm^{-3}). The dead layer thicknesses are very similar in both cases (32 and 35 Å). The dead layer is responsible for the slight downward dispersion observed at the lowest electron energies (<20 eV) in the 500-eV curve. It should be noted that because of the simplified nature of the three-layer model, these layer thicknesses are approximate values, despite the strong sensitivity of the simulations to the actual values. It is also important to note that the semi-infinite ''bulk'' region of the model does not actually represent the true bulk zinc concentration (on a depth scale of several micrometers) because of the limited probing depth.

Clearly, the region of very high carrier concentration produced by the IBA procedure and subsequent dopant diffusion extends somewhat deeper for ion bombardment at 2 keV than at 500 eV (49 Å cf. 33 Å). However, both of these mid-layer thicknesses derived from the HREELS measurements are much smaller than the overall damage diffused region, which in n-type InAs is estimated to be at least 400 Å.[10] They are closer to the typical amorphization depths (several tens of angstroms) found in III–V materials following ion sputtering at ion energies of several hundred eV.[20] It is possible that zinc diffusion into the amorphized surface region of the material controls the formation of this region of the highest hole concentration. Of course, the HREELS measurements reported here only detect the presence of holes, not the corresponding electron acceptors (Zn^- ions) or neutral Zn atoms.

B. 2D electron plasmon modes

The energy of a 2D plasmon increases as the square root of its wave vector,[4] and the dispersion as a function of electron energy E_i in dipole HREELS can be calculated as

$$\omega_{2D}=\frac{n_{2D}e^2\sin\theta_i}{\varepsilon_0\varepsilon(\infty)m^*}\sqrt{\frac{m_e}{2E_i}}, \tag{3}$$

where n_{2D} is the sheet electron density and θ_i is the electron incidence angle (45° in these experiments). For the inversion layer system at the InAs (001) and (111) surfaces, the sheet charge density can be equated to the donorlike surface-state density. This is known to be dependent on the surface reconstruction[13,14,17] and for InAs (001)-(4×2) and (111)A-(2×2) surfaces, it is approximately 4×10^{11} cm^{-2} and 8×10^{11} cm^{-2}, respectively.[12] For the (001) surface, the 2D plasmon frequency varies between 2 and 9 meV in the electron energy range explored experimentally, while the corresponding range on the (111) surface is 9–34 meV. The HREEL spectra from the (001) surfaces show only a small degree of elastic peak broadening, which is consistent with the calculated 2D plasmon frequencies. This allows the inversion layer to be treated as a ''dead layer'' without affecting the higher loss region of the spectra. The width of the inversion layer can be estimated in the Fang-Howard approximation by calculating the extent of the ground-state wave function perpendicular to the surface, z_{GS}

$$z_{GS}=\int_0^\infty z\psi^2(z)dz. \tag{4}$$

Using reasonable values for the surface Fermi level derived from previous work[12,17] the calculation produces a depth of 21 Å. The values for the dead layer thickness, derived from the HREELS simulations, appear highly plausible in light of this value.

For the (111) surfaces, the 2D plasmon frequencies are significantly greater than for the (001) surfaces, and at low electron incidence energies they are sufficient to allow the 2D plasmon to couple with the optical phonon ($\omega_{TO}=27$ meV) to produce plasmaron modes of mixed character.[21] This explains why a distinct phonon peak is not observed on the (111) surfaces even at the lowest electron energy (Fig. 2). It also explains the electron energy dependence of the elastic peak broadening for the (111) surfaces, which is greater at lower electron energies (Fig. 2) due to the higher 2D plasma frequency.

C. Hole plasmon modes

Some insight into the two-component plasma model can be gained by solving the surface loss equation $\varepsilon(\omega)=-1$ for a highly simplified system.[1] The optical phonons are neglected, as is the plasmon damping and (initially) the spatial structure of the substrate. For this uniform semi-infinite medium, the assumed dielectric function is

$$\varepsilon(\omega)=\varepsilon(\infty)\left[1-\frac{\omega_1^2}{\omega^2-\beta_1^2q^2}-\frac{\omega_h^2}{\omega^2-\beta_h^2q^2}\right], \tag{5}$$

which represents the essential features of the plasma part of the full dielectric function given in Eq. (1). We also use the approximation $\varepsilon(\infty)\gg1$.

In the absence of spatial dispersion ($\beta_i=0$), the surface loss equation predicts only one plasmon mode, which is nondispersive and has a frequency ω_{OP} given by

$$\omega_{OP}=\sqrt{\omega_1^2+\omega_h^2}. \tag{6}$$

This value is close to the heavy-hole plasma frequency for a system in which $m_{lh}\ll m_{hh}$. This optical plasmon mode consists of the light and heavy holes oscillating out of phase. However, if spatial dispersion is retained, the surface loss equation predicts a frequency for the optical mode given by

$$\omega=\sqrt{\omega_{OP}^2+\beta_{OP}^2q^2}, \tag{7}$$

where the optical spatial dispersion coefficient β_{OP} is

$$\beta_{OP}^2=\frac{(\beta_h^2-\beta_1^2)(\omega_1^2-\omega_h^2)}{\omega_{OP}^2}\approx\beta_1^2. \tag{8}$$

In the hydrodynamic model, this spatial dispersion arises from the finite compressibility of the carrier ''fluids:'' at short wavelengths the increased compression raises the excitation energy.[22] The model predicts an additional dispersion term which is quartic in the wave vector, neglected in the long-wavelength regime considered here. In addition, since $m_{lh}\ll m_{hh}$ in the InAs system, the optical dispersion parameter reduces to the light-hole dispersion parameter as shown in Eq. (8), the dominant term being $(\beta_l\omega_h)^2$. For an ideal p-type InAs sample, at room temperature and with a doping level of 1×10^{19} cm^{-3}, the optical plasmon dispersion coef-

ficient is nearly identical to the light-hole dispersion coefficient (both 0.74×10^6 ms^{-1}). The resulting upward dispersion with increasing wave vector indicated by Eq. (7) is similar to that of the single component plasma.[3,17] Upward dispersion with increasing wave vector (decreasing electron energy) is observed in the simulated and experimental spectra (Figs. 2 and 4) although the changes of probing depth through the highly inhomogeneous hole distribution also contribute to the dispersion.

For completeness, we will now briefly discuss the acoustic plasmon mode, for which the light and heavy holes oscillate in phase. This mode has the following simple linear dispersion relation:

$$\omega=\beta_{\mathrm{AC}}q, \tag{9}$$

where in the two-oscillator model the acoustic dispersion coefficient β_{AC} is given by

$$\beta_{\mathrm{AC}}^2=\frac{\beta_1^2\omega_h^2+\beta_h^2\omega_1^2}{\omega_{\mathrm{OP}}^2}\sim\beta_1^2. \tag{10}$$

The acoustic plasmon dispersion coefficient derived by this method is very similar to that described by Ruvalds[22] which was obtained using the random-phase approximation (RPA) in the limit $m_{\mathrm{lh}}\ll m_{\mathrm{hh}}$ (an assumption not essential in the above discussion). If $m_{\mathrm{lh}}\ll m_{\mathrm{hh}}$ then the light-hole dispersion term $(\beta_l\omega_h)^2$ tends to dominate Eq. (10), in agreement with the RPA coefficient which depends only on the Fermi velocity of the lighter carriers. Of course, the above considerations do not account for damping, which is thought to be a critical factor in the behavior of acoustic plasmons.[22] However, it should be noted that a strict ''low damping'' condition ($\Gamma\ll\omega$) is not necessary for the observation of a mode in HREELS; indeed, in the simulation curves shown in Fig. 3, the damping value (350 meV) is greater than the plasmon frequencies.

Despite its linear dispersion, it may still be possible to observe an acoustic plasmon in specular HREELS due to distortion of the ''ideal'' dispersion relation by changes in the probing depth through an inhomogeneous sample. In practice, this means having additional upward dispersion at low probing depths (i.e., a higher spatial dispersion coefficient closer to the surface) since the phase velocity of the acoustic plasmon is typically lower than the phase velocity at the peak of the surface loss function. δ-doped layers in particular represent a highly inhomogeneous charge distribution which may produce such an effect, and an experimental study of p-type δ-doped GaAs has been carried out by Biagi and del Pennino.[4] With a moderate dopant concentration in the delta layer (3×10^{13} cm^{-2}) they observed 2D plasmon behavior as an electron energy-dependent asymmetric broadening of the elastic peak. The δ layer was modeled as a thin hole gas, using only a *single* Drude term for the optical plasmon (therefore neglecting acoustic modes). We have performed some theoretical calculations with idealized systems to gauge the importance of acoustic plasmons in specular HREELS of highly inhomogeneous p-type materials.

We consider a two-layer system where the bulk dielectric function ε_b is given simply by $\varepsilon_b=\varepsilon(\infty)$ and the surface layer (of thickness d) has a dielectric function ε_s given by

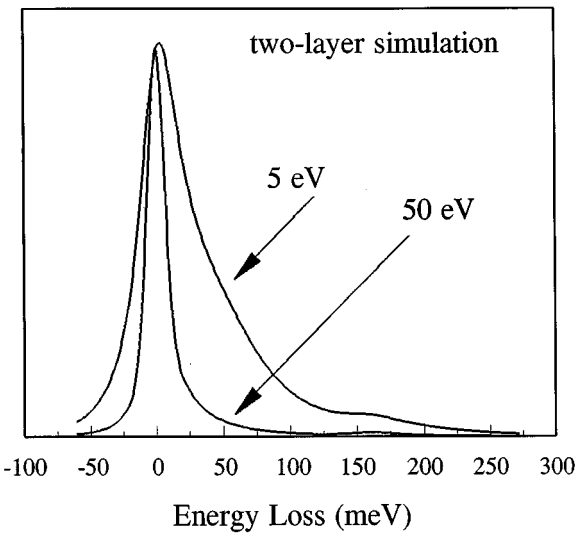

FIG. 7. Simulated specular HREEL spectra based on the simplified two-layer model described by Eq. (11), using electron energies of 5 and 50 eV. The plasma slab thickness is 10 Å and the heavy- and light-hole plasma frequencies are 160 and 40 meV, respectively.

$$\varepsilon_s=\varepsilon(\infty)\left[1-\frac{\omega_h^2}{\omega^2}-\frac{\omega_1^2}{\omega^2-\beta_1^2q^2}\right]. \tag{11}$$

This represents a simplified two-component plasma slab for which dispersion is important only in the light-hole component, and the optical phonons are also omitted for simplicity. Two simulated specular HREEL spectra are shown in Fig. 7 for this system at electron energies of 5 and 50 eV. The heavy-hole plasma frequency is set at 160 meV and the plasma slab thickness is 10 Å, while the light-hole plasma frequency is set at 40 meV (appropriate to InAs as shown in Fig. 5). At 50 eV, the elastic peak is not broadened significantly, and a weak plasmon peak is observed close to 160 meV. This peak is due to the optical 3D hole plasmon mode. At 5 eV, there is striking asymmetric peak broadening on the elastic peak, and the 3D mode peak has shifted downward by around 10 meV. The downward dispersion of the 3D mode with increasing electron energy is due to the increased probing depth. The increase of the elastic peak broadening with increasing wave vector is consistent with both 2D plasmon modes and structure-induced acoustic modes.

This two-layer system can be solved analytically using the equations derived by Ibach and Mills,[1] the algebra being straightforward if somewhat laborious. The optical mode (neglecting its native spatial dispersion) has a frequency modified by the presence of the slab structure according to

$$\omega^2=\frac{\omega_h^2}{2}\left[1+e^{-2qd}\right]. \tag{12}$$

The exponential factor represents the effects of the changing probing depth as the wave vector is altered. In the limit of a thick slab, the heavy-hole plasma frequency is recovered, while for a thin slab the dispersion becomes proportional to the square root of the wave vector, i.e., the expected 2D plasmon behavior appears.[4] However, for the acoustic

mode, the dispersion is *not* affected by the finite thickness of the slab, due to a cancellation of all the exponential factors. The linear dispersion relation is unaffected by the slab structure, and therefore even for such an inhomogeneous system, the acoustic mode does not appear in specular HREEL spectra. We therefore assign all of the low-energy intensity on the loss side of the elastic peak in Fig. 7 to 2D plasmons. In fact, there is direct evidence for this from the simulations, since the shape of the spectra in the low-energy-loss region is nearly independent of the light-hole spatial dispersion coefficient. This would not be the case for acoustic plasmons, whose frequency depends critically on the light-hole dispersion parameter. We investigated several other inhomogeneous space-charge structures in a similar manner and found no loss features with behavior compatible with acoustic plasmon modes. This implies that such modes can in general be neglected in specular HREELS confirming the validity of the assumption made by Biagi and del Pennino.[4]

VI. CONCLUSIONS

Surface-plasmon modes in Zn-doped *p*-type InAs(001) and InAs(111) have been investigated using HREELS. The 2D electron plasmon modes were observed as a broadening of the elastic peak, with the higher surface electron density of the (111) surface producing greater broadening. Optical hole plasmon modes were observed on samples prepared by ion bombardment and annealing (IBA), but not on those prepared by AHC. It has been shown that IBA causes rapid diffusion of the Zn acceptors into the near-surface region, producing highly nonuniform hole distributions with densities in the range $1\times10^{18}\,\mathrm{cm}^{-3}-4\times10^{19}\,\mathrm{cm}^{-3}$. The highest hole densities are associated with increased ion-induced defect concentrations caused by near-normal ion incidence and high ion energies, in agreement with previous HREELS studies of ion-beam-induced damage in InAs and InSb.[10,19] In contrast, AHC produces no such dopant diffusion. The dielectric theory and a three-layer model for the hole distribution near the surface were successfully employed to model the HREEL spectra and plasmon dispersion. The two-component plasma was modeled using two plasma oscillators incorporating spatial dispersion. Further calculations were made using this two-component model and it was established that acoustic plasmons play no role in specular HREEL spectra even for highly inhomogeneous charge distributions.

ACKNOWLEDGMENTS

Financial support for this work was provided by the Engineering and Physical Sciences Research Council (EPSRC), UK, under Contract No. GR/J83543. We gratefully acknowledge the support of The Royal Society for the provision of a research Grant (No. RSRG/16236) and thank Dr. A. P. Mowbray of MCP Wafer Technology, UK, for helpful discussions.

*Author to whom correspondence should be addressed. FAX: +44-1203-692-016. Electronic address: C.F.McConville@warwick.ac.uk

[1] H. Ibach and D. L. Mills, *Electron Energy Loss Spectroscopy and Surface Vibrations* (Academic, New York, 1982).
[2] H. Lüth, Surf. Sci. **126**, 126 (1983).
[3] T. S. Jones, M. O. Schweitzer, N. V. Richardson, G. R. Bell, and C. F. McConville, Phys. Rev. B **51**, 17 675 (1995).
[4] R. Biagi and U. del Pennino, Phys. Rev. B **50**, 7573 (1994).
[5] U. del Pennino, R. Biagi, and C. Mariani, Appl. Surf. Sci. **56**, 44 (1992).
[6] Y. Meng, J. Anderson, and G. J. Lapeyre, Phys. Rev. B **45**, 1500 (1992).
[7] R. Biagi, C. Mariani, and U. del Pennino, Phys. Rev. B **46**, 2467 (1992).
[8] E. F. Schubert, *Doping in III-V Semiconductors* (Cambridge University Press, Cambridge, England, 1993), and references therein.
[9] G. R. Bell, N. S. Kaijaks, R. J. Dixon, and C. F. McConville (unpublished).
[10] G. R. Bell, C. F. McConville, and T. S. Jones, Appl. Surf. Sci. **104/105**, 17 (1996).
[11] G. R. Bell and C. F. McConville, Appl. Phys. Lett. **69**, 2695 (1996).
[12] G. R. Bell, T. S. Jones, and C. F. McConville, Surf. Sci. (to be published).
[13] L. Ö. Olsson, C. B. M. Andersson, M. C. Håkansson, J. Kanski, L. Ilver, and U. O. Karlsson, Phys. Rev. Lett. **76**, 3626 (1996).
[14] M. Noguchi, K. Hirakawa, and T. Ikoma, Phys. Rev. Lett. **66**, 2243 (1991).
[15] *Semiconductors Physics of Group IV Elements and III-V Compounds*, edited by K.-H. Hellwege, and O. Madelung, Landolt-Börnstein, New Series, Group III, Vol. 17, Pt. a (Springer-Verlag, Berlin, 1982).
[16] Ph. Lambin, J. P. Vigneron, and A. A. Lucas, Comput. Phys. Commun. **60**, 351 (1990).
[17] G. R. Bell, C. F. McConville, and T. S. Jones, Phys. Rev. B **54**, 2654 (1996).
[18] G. R. Bell, C. F. McConville, C. P. A. Mulcahy, and T. S. Jones, J. Phys. Condens. Matter **9**, 2903 (1997).
[19] T. S. Jones, M. Q. Ding, N. V. Richardson, and C. F. McConville, Surf. Sci. **247**, 1 (1991).
[20] J. B. Malherbe, Crit. Rev. Solid State Mater. Sci. **19** (2), 55 (1994); **19**, (3), 129 (1994).
[21] H. Yu and J. C. Hermanson, Phys. Rev. B **40**, 11 851 (1989).
[22] J. Ruvalds, Adv. Phys. **30**, 677 (1981).